

Alignment of high-aspect ratio colloidal gold nanoplatelets in nematic liquid crystals

Julian S. Evans, Corinne N. Beier, and Ivan I. Smalyukh^{a)}

Department of Physics, Renewable & Sustainable Energy Institute, and Liquid Crystal Materials Research Center, University of Colorado, Boulder, Colorado 80309, USA

(Received 20 March 2011; accepted 27 June 2011; published online 12 August 2011)

We study elasticity-mediated alignment of anisotropic gold colloids in liquid crystals. Colloidal gold particles of controlled shapes (spheres, rods, and polygonal platelets) and sizes are prepared using well-established biosynthesis techniques with varying solvent conditions. When introduced into liquid crystalline structured solvents, these gold particles impose tangential or vertical surface boundary conditions for the liquid crystal molecules or building blocks such as chromonic molecular aggregates. This allows for multiple types of their controlled alignment in both lyotropic and thermotropic liquid crystals and is of interest for self-assembly-based fabrication of tunable nanostructured composite materials. © 2011 American Institute of Physics. [doi:10.1063/1.3620550]

I. INTRODUCTION

Composite materials comprised of nano-sized and micro-sized colloidal particle dispersions in structured host media have attracted a great amount of interest.^{1–10} The plasmonic properties of noble metallic particles make them desirable structural units of a number of novel composites such as optical metamaterials.^{11–14} In these artificial materials, which are also often referred to as “left-handed materials,”^{11–14} ordered structures of predesigned anisotropic nanoparticles play the role of “building blocks,” similar to that of molecules and atoms in conventional matter,¹³ allowing for the engineering of unprecedented properties not encountered in naturally occurring materials,¹⁴ such as negative refractive index. Control of the particle shape and size is essential for engineering the needed surface plasmon resonance properties for the development of optical and near-infrared metamaterials. The synthesis of functionalized spheres through thiol linkages,¹⁵ the seed-mediated growth of nanorods,¹⁶ and a variety of polyhedral and platelet-shaped¹⁷ particle syntheses are well understood and broadly used, although obtaining micro-sized gold colloids through conventional wet chemical synthesis is limited by the high density of gold (causing sedimentation of larger particles due to gravity) and is rarely accomplished.^{15–21} Previous studies have shown that aqueous solutions of a variety of polyol containing biological materials such as aloe vera extract,¹⁸ bovine serum albumin,¹⁹ lemon grass extract,²⁰ and cellulose²¹ provide effective means for obtaining gold triangular platelets of various lateral sizes and thicknesses. The post-synthetic manipulation of morphology has been previously described in the context of a many-particle to one-particle transformation through lengthy refluxing.²² However, the potential uses of biosynthesized gold nanoparticles to form tunable and reconfigurable nanostructured composites have not been explored. This is despite the fact that they are of particular interest for such applications because of the simplicity of synthesis and

the feasibility of obtaining nanoparticles with a broad range of controlled shapes and sizes.

In this work, we report dispersion of high-aspect ratio biosynthesized gold platelets in both thermotropic and lyotropic liquid crystals (LCs). We manipulate the particles' shapes and sizes through redispersion in different solvents and show that the gold platelet particles can impose both tangential and vertical surface boundary conditions for the liquid crystalline molecular alignment. This allows for several different types of elasticity-mediated self-alignment of polygonal gold platelets in LC host fluids, which are of interest and importance for both fundamental and applied research on LC colloidal dispersions.

II. MATERIALS AND METHODS

A. Preparation of gold nanoparticles

A typical gold particle synthesis was performed by dissolving 3.9 mg of gold(III) chloride hydrate in 9 mL of the solvent, adding 1 mL of aqueous aloe vera extract solution, and leaving the mixture at room temperature overnight. Aloe vera extract was prepared by finely cutting 30 g of a 2 lb aloe vera leaf (obtained from Aloe Farms, Inc.) and boiling it in 100 mL of de-ionized water. According to previous studies, the reductant necessary for the nanoparticle synthesis is likely a hydrophilic aldose, or aldehyde, or ketone present in aloe vera.¹⁷ The solvents used and the gold(III) chloride hydrate were obtained from Sigma Aldrich and used without further purification except for the de-ionized water which was obtained from the Barnstead/Thermolyne E-pure system (>17 MΩ cm).

During the nanoparticle synthesis, we used water as the solvent to produce 300 nm × 5 nm triangles and hexagons [Figs. 1(a) and 1(b)], following the procedure previously reported by Sastry *et al.*^{18,20} Using toluene instead of water produces 150 nm spheres [Fig. 1(d)] and using ethanol produces 2 μm by 300 nm rods [Fig. 1(e)]. Using methanol as the solvent produces highly polydisperse triangles, hexagons, and nonagons [Fig. 2(a)] with 5 nm thickness [Figs. 2(b) and

^{a)}Electronic mail: Ivan.Smalyukh@Colorado.edu.

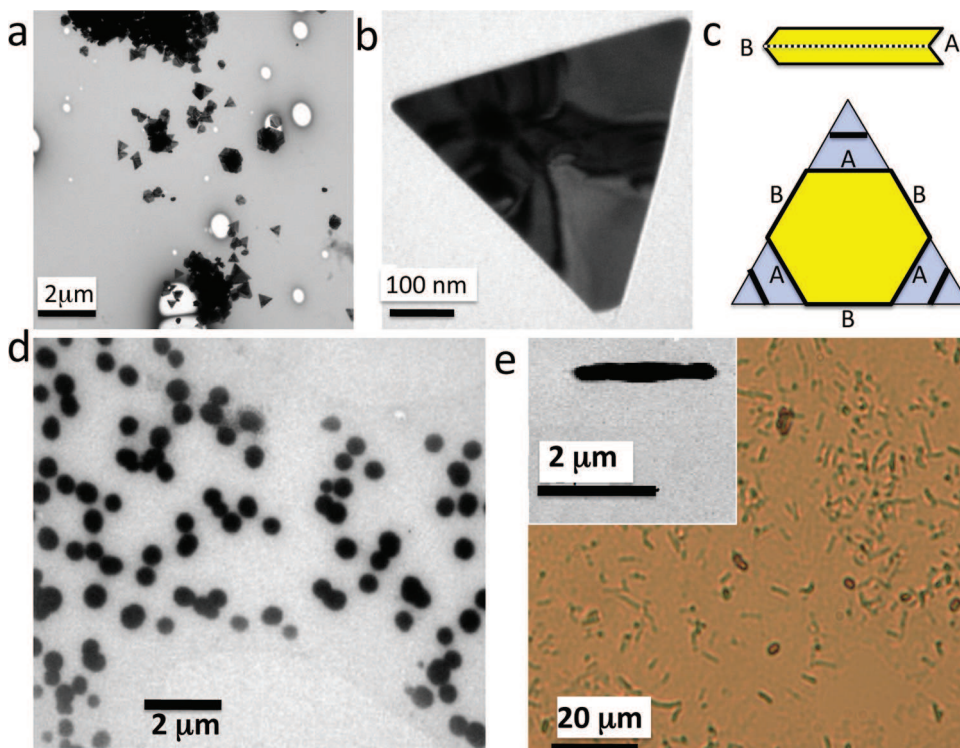


FIG. 1. (Color online) Triangular colloidal platelets synthesized using aloe vera and gold(III) chloride hydrate and water, toluene, or ethanol as solvents. (a) A large-area image showing colloidal triangles of about 300 nm in the lateral dimensions, along with a smaller number of particles of other polygonal platelet shapes and of different sizes obtained by the use of water as a solvent. (b) A magnified image of a 300 nm triangular platelet similar to the ones shown in (a). (c) A schematic showing the single twin growth mechanism responsible for the formation of the triangular platelets; the concave and convex edges of the platelet are marked with “A” and “B,” respectively. The gray regions and lines illustrate the kinetics of the nanoparticle growth process. (d) Colloidal spheres about 150 nm in diameter grown in toluene. (e) Colloidal gold rods of about two micrometers in length, grown in ethanol.

2(c)] and side lengths up to 10 microns. These platelets appear to be relatively rigid in solution since thermal fluctuations of their shape (when dispersed in a solvent) are not readily observable. Triangular platelets are formed when there is one twinning plane parallel to the plane of the platelet resulting in one set of fast growing concave edges denoted by “A” in Fig. 1(c), following the silver halide model.^{17,23} Hexagonal platelets are the result of two twinning planes yielding more highly symmetric growth^{17,23} [Fig. 2(e)]. The nonagons are likely the result of particle growth with three twinning planes producing one doubly concave edge and one singly concave edge [Fig. 2(f)]. In the primary growth phase the doubly concave edge grows faster, which results in an asymmetric hexagonal shape [Fig. 2(c)]. Upon filling the original concavities the doubly concave edges become singly concave [Fig. 2(g)], which allows for a secondary growth that produces the final nonagon shape [Fig. 2(d)]. This secondary growth is occurring only from the central twinning plane; it does not follow the overall crystallography of the particle and can result either in relatively small triangular platelet growths off of three sides [Fig. 2(c)], or proceed further to produce nonagons, or go to completion to produce non-equilateral hexagons [see the inset of Fig. 2(d)]. The simple replacement of water with less polar solvents in these well understood biosynthesis procedures results in dramatic and robust changes of the obtained particle shapes and sizes.

B. Characterization

Transmission electron microscopy (TEM) imaging samples are prepared by pipetting 2 μl of solution onto a Formvar-coated copper grid. The TEM characterization is performed using a Philips CM10 system with an accelerating

voltage of 80 kV. For the atomic force microscopy (AFM) imaging, the samples are prepared by drying 2 μl of the solution on a silica wafer. The AFM images are obtained using a Digital Instruments’ Nanoscope III with non-conductive silicon nitride contact mode tips from Veeco (model MLCT-AUHX). The vertical displacement profiles are measured using AFM in the contact imaging mode. For example, representative AFM images of gold platelets reveal that their thickness is about 5 nm [Figs. 2(a) and 2(b)]. Optical images are obtained in bright field and polarizing imaging modes using the Olympus BX51 upright polarizing optical microscope. To obtain optical micrographs, we also use the Spot 14.2 Color Mosaic Camera (from Diagnostic Instruments, Inc.) and microscope objectives with magnifications of 10, 20, and 50 \times of numerical aperture, NA = 0.1–0.5 (Olympus). For optical imaging, dispersions of particles are either dried on glass microscope slides or directly imaged in the dispersions in the bulk of the glass cells. The scanning electron microscopy (SEM) samples are prepared by drying 5 μl of the dispersion on a silica wafer. The SEM images were taken by the use of the JSM-6480LV SEM operating in high vacuum mode with 5 kV accelerating voltage.

C. Liquid crystal sample preparation

The studied samples were designed to probe the alignment of gold nanoparticles in the bulk and at the surfaces of both thermotropic and lyotropic liquid crystals. The room-temperature thermotropic nematic LC mixture, E31, was purchased from EM Industries and used as supplied. The lyotropic chromonic LCs are formed by solutions of cromolyn (from Sigma, purified by the use of filters with a pore size of 0.2 μm) in de-ionized water at 13–14 wt. % to insure a room-temperature nematic phase. By means of solvent

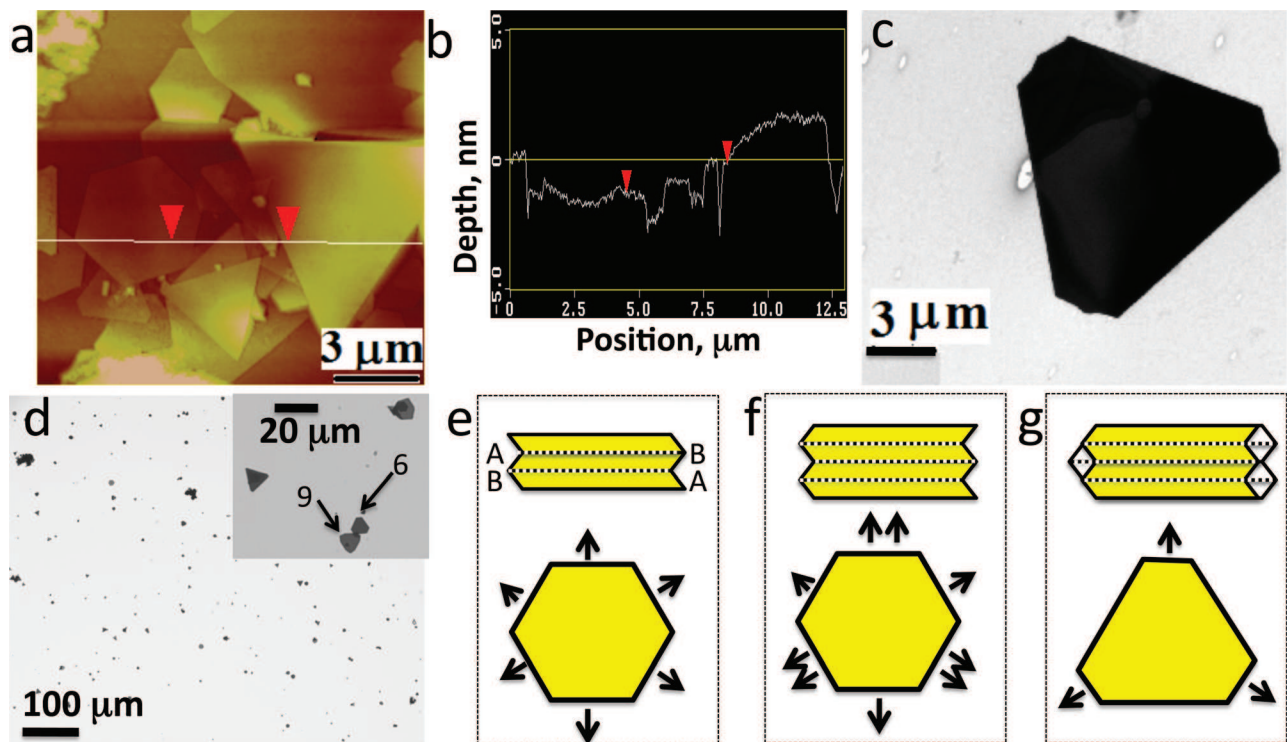


FIG. 2. (Color online) Colloidal platelets obtained by the use of methanol as a solvent. (a) An AFM image of the surface profile, and (b) the depth profile across the platelets indicate that the polygonal particles are about 5 nm in thickness. (c) Enlarged image of a colloidal platelet. (d) Optical micrograph showing predominantly colloidal triangles (with some hexagons and nonagons) obtained after drying the dispersion on a glass cover slide. Schematic illustrations of the (e) double-twinned growth mechanism of hexagons, (f) triply twinned primary growth mechanism of non-equilateral hexagons, and (g) secondary growth on triply twinned particles that yields nonagons or non-equilateral hexagons.

drying and solvent exchange, the polygonal platelets are introduced into the thermotropic nematic LC mixture, E31, and the water-based lyotropic chromonic LC mixture.

To study gold nanoparticles in the LC bulk, the glass cells are prepared using 1 mm-thick plates separated by spherical spacers to set the cell gap within the range of 10–20 μm and sealed using epoxy. The glass cells are then infiltrated with LC dispersions using capillary action. For vertical (homeotropic) surface alignment of the director of thermotropic LCs, we treat confining substrates of the cells with [3-(trimethoxysilyl)propyl]octadecyl-dimethylammonium chloride (obtained from Aldrich). The other cells were formed using plasma-cleaned glass plates without further treatment.

In the experiments designed to probe the platelet alignment at the LC surfaces, 5 μl of an aqueous dispersion of polygonal platelets is placed atop a thin layer of glycerol (obtained from Aldrich) so that, after water-glycerol mixing, some particles are trapped at the glycerol-air interface with the orientation of their large-area faces parallel to the interface. Upon placing a 2 μl droplet of E31 atop the glycerol, the platelets remained confined at the LC-glycerol interface and their alignment and stability was explored using optical microscopy.

III. RESULTS AND DISCUSSION

A. Self-alignment of anisotropic nanoparticles in liquid crystals

The biosynthesized polygonal platelets impose vertical boundary conditions for the thermotropic nematic LC director.^{24–30} In a homeotropic cell of E31, the colloidal platelets

align with their large-area faces orthogonally to the vertical (homeotropic) far-field director, as shown in Fig. 3 for the case of a triangular particle. A particle induces a disclination loop encircling it in the plane of the platelet. In some places around the platelet, the defect loop is pinned to the platelet's edge, thus transforming into a surface disclination, and then becoming a bulk defect line again. The details of director distortions around such a platelet will need to be explored further, however, experiments suggest that the observed defect line is a half-integer disclination of strength $s = -1/2$ as shown in the schematic drawing in Fig. 3(d). A similar disclination loop, also known as a “Saturn ring” defect line,² can be observed around spherical particles with vertical boundary conditions.^{2,30} Because of the homeotropic surface anchoring, the alignment of the thin gold platelet with the large-area faces orthogonally to the far-field director and the observed disclination loops are expected to correspond to the minimum-elastic-energy alignment and director structure. Since the normal vector of the platelet plane is parallel to director field $\mathbf{n}(\mathbf{r})$, the induced director distortions ideally have the D_N symmetry of the polygonal platelet with N edge faces. However, the spontaneous pinning of the defect line to the edge faces of the platelet may break the D_N symmetry. This spontaneous formation of topological defect lines around the colloids could lead to qualitatively different elasticity- and defect-mediated modes of colloidal self-assembly than those seen for platelets with tangential boundary conditions^{25,26} and spherical particles.^{1,2,27} From the elastic energy standpoint, the orientations of the gold triangular platelets with the induced distortions around them are invariant

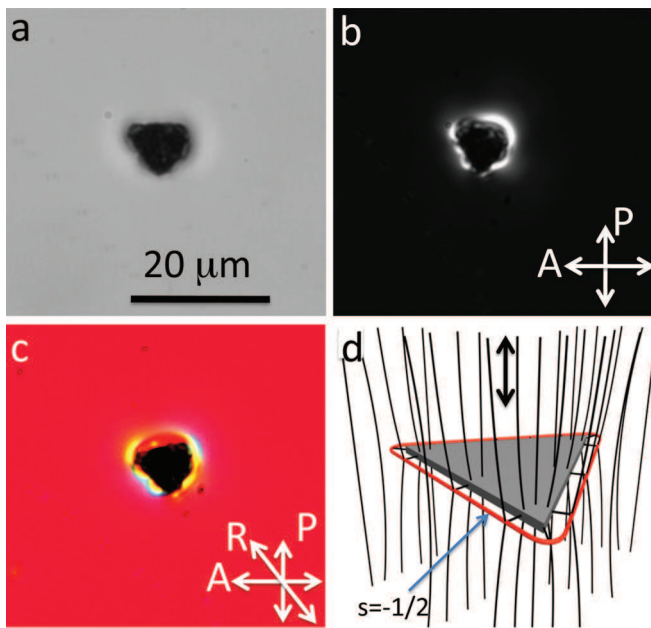


FIG. 3. (Color online) Triangular platelet of gold in the bulk of a thermotropic nematic LC mixture E31. (a)–(c) Co-located optical microphotographs of a triangular platelet in a homeotropic LC cell filled with E31 obtained in: (a) bright-field transmission microscopy mode, (b) polarizing microscopy mode between crossed polarizer labeled as “P” and analyzer labeled as “A,” and (c) polarizing microscopy mode with an additional retardation plate with the fast axis labeled “R” inserted at 45° between the crossed polarizers. (d) A schematic showing the $\mathbf{n}(\mathbf{r})$ -structure around a triangular platelet encircled by a loop of a disclination of strength $s = -1/2$; the platelet self-aligns orthogonally to the far-field LC director marked by a black double arrow.

with respect to rotations around an axis parallel to the far field director and orthogonal to the platelet’s large-area faces.

The alignment of similar gold platelets in a lyotropic chromonic LC has qualitatively different features from that in a thermotropic LC discussed in the preceding text (Fig. 4): (a) bulk defects around the particles are not observed, and (b) boundary conditions for $\mathbf{n}(\mathbf{r})$ imposed by platelet surfaces are tangential. The observation of many particles in a sample with non-uniform texture and director distortions on scales much larger than the size of the particles leads to the conclusion that thin triangular platelets [Fig. 4(a)] align with the large-area faces parallel to the far-field director, barely perturbing local $\mathbf{n}(\mathbf{r})$ at their edges [Fig. 4(b)]. Although the system of a platelet nanoparticle in the LC does not have rotational symmetry with respect to the normal to the large-area faces of the platelet, the elastic energy cost of director distortions at the edge faces of 5 nm-thick platelets is relatively small. Therefore, the observed rotations of such a platelet around the axes [marked by red double arrows as shown in Fig. 4(a)] preserve the alignment of the large-area faces parallel to the far-field director [black double arrow in Fig. 4(a)] but show no specific alignment of the edge faces with respect to the far-field director. This is likely due to the fact that the changes of the bulk elastic and surface anchoring energies associated with the rotations of such a 5 nm-thick platelet around the normal to the large-area faces are comparable or smaller than the thermal energy.

A schematic in Fig. 4(c) shows a thicker triangular platelet with edge faces inducing well-defined boundary

conditions for the $\mathbf{n}(\mathbf{r})$: the orientations that minimize the overall free energy require the large-area faces and one edge face aligning parallel along the $\mathbf{n}(\mathbf{r})$, which is similar to the case of our previous studies on lithographically generated polygonal platelets.²⁵ The ensuing $\mathbf{n}(\mathbf{r})$ -distortions have dipolar symmetry dictated by the boundary conditions at the surfaces of the faceted particle with low-symmetry shape.²⁵ The elastic dipole moment of a structure shown in Fig. 4(c) is aligned orthogonally to the far-field director and its orientation is invariant with respect to the rotations around the axis parallel to the far-field director and one edge face. Although an instantaneous elastic dipole can also be defined for the structure shown in Fig. 4(a), its orientation with respect to the far-field director is not stable, unlike in the case of the other dipolar structure shown in Fig. 4(c). The experimental optical micrographs shown in Figs. 4(d)–4(f) suggest that both strongly and weakly aligned triangular platelets [Figs. 4(c) and 4(a), respectively] can be observed in the very same lyotropic LC sample. To generalize these observations and the analysis of particles of other shapes, polygonal gold platelets with an even number of edge faces (hexagons) are expected to induce quadrupolar distortions of $\mathbf{n}(\mathbf{r})$, while the ones with an odd number of edge faces (triangles and nonagons), induce dipolar distortions. This is reminiscent of the behavior of lithographically generated polygonal platelets that we studied previously,^{25,26} however, the ability of inducing homeotropic surface boundary conditions for $\mathbf{n}(\mathbf{r})$ (in addition to tangential ones) along with much larger aspect ratios of the platelet’s lateral sizes to their thickness, allows one to achieve several new types of platelet alignment in the LC bulk with respect to the uniform far-field director, as shown in Figs. 3 and 4. The thicker platelets interact with elastic distortions in unaligned LC samples [Figs. 4(d)–4(f)], which may provide the means for their spatial patterning in LCs by use of deliberately introduced elastic distortions by means of surface treatment and topography, external fields, light, etc.

An interesting open question is whether the elasticity-mediated forces between platelets (due to the elastic distortions that they induce) can be utilized for colloidal self-assembly. Because of the small thickness of the gold platelets, both dipolar and quadrupolar elastic interaction between platelets of different shapes having tangential surface anchoring are expected to be weak, overcoming thermal fluctuations only at small distances. This is due to the weak elastic distortions induced by such thin particles, which is reminiscent of the weak elastic interactions between rod-like nanoparticles previously studied.²⁸ Consequently, self-assembled structures of such aligned polygonal platelets in the studied LCs are not observed [Figs. 4(b), 4(e), and 4(f)]. Since biosynthesized gold triangular platelets reported in the literature have thicknesses of 3–8 nm when obtained using aloe vera,¹⁸ 15–20 nm when using lemon grass²⁰ and bovine serum albumin,¹⁹ and 200–800 nm when using cellulose,²¹ their dispersions in chromonic LCs is a good system for exploring how inter-particle interactions and their self-assembly depend upon the thickness and aspect ratio of these platelets.

The platelets found at the interface of glycerol and thermotropic LC E31 impose tangential surface boundary

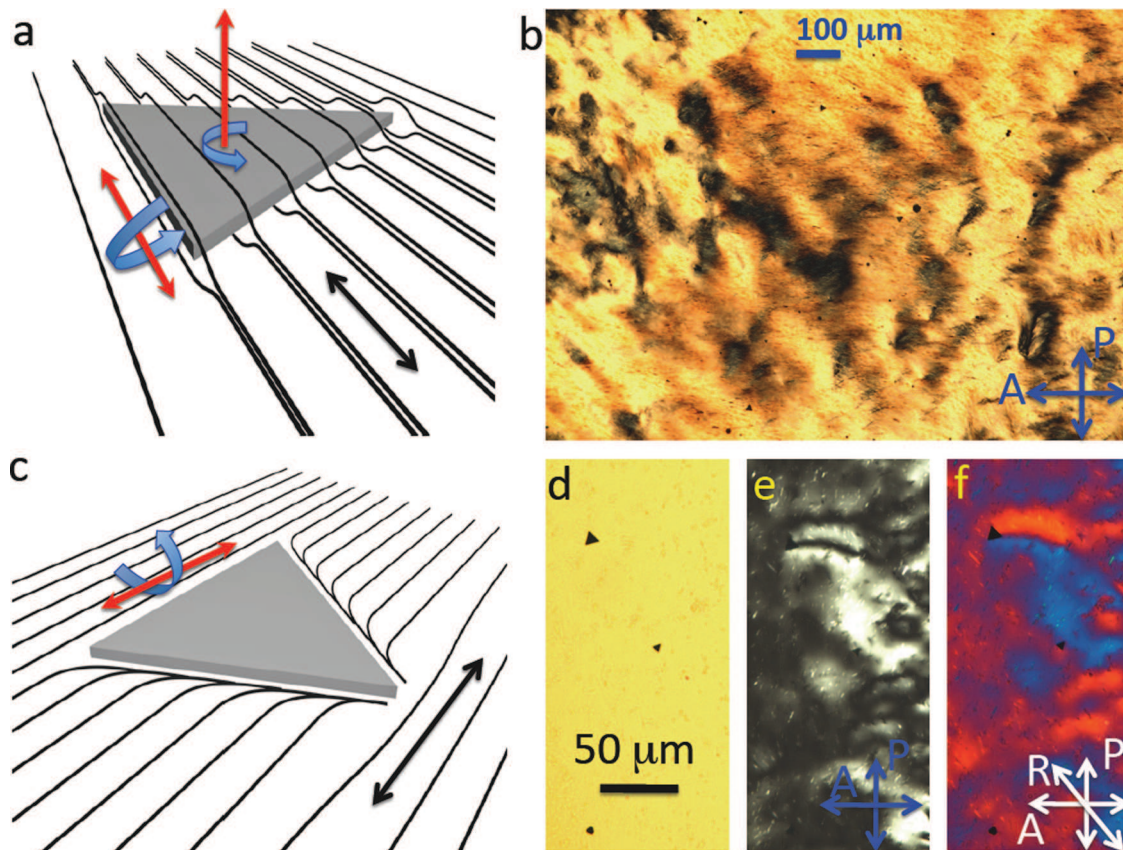


FIG. 4. (Color online) Gold polygonal platelets of varying lateral size and thickness in a lyotropic chromonic LC of the aqueous solution of cromolyn. (a) A schematic illustration showing a thin triangular platelet aligning with the large-area faces parallel to the far-field director and barely perturbing the director field at its edge faces; the allowed rotations of the platelet around the axes marked by red double arrows preserve the alignment of the large-area faces parallel to the far-field director (marked by the black double arrow). (b) Polarizing microscopy texture of the LC-sample with non-uniform $\mathbf{n}(\mathbf{r})$ obtained between crossed polarizer “P” and analyzer “A,” and showing polygonal platelets at orientations having large-area faces following $\mathbf{n}(\mathbf{r})$. (c) A schematic showing a triangular platelet with edge faces inducing a well-defined tangential surface anchoring; the orientations that minimize the overall free energy require that the large-area faces and one edge face align parallel to $\mathbf{n}(\mathbf{r})$. (d), (e), and (f) Transmission optical microscopy images obtained in (d) bright field mode, (e) and (f) polarizing microscopy modes with (e) crossed polarizer and analyzer, and (f) with an additional retardation plate (having fast axis marked “R”) between the polarizers; the images show that the largest platelet is co-located with the deformed $\mathbf{n}(\mathbf{r})$ while the two smaller ones do not induce detectable distortions of $\mathbf{n}(\mathbf{r})$, similarly to the schematics shown in (c) and (a), respectively.

conditions for the director at the large-area faces (Fig. 5). This is a likely consequence of the platelets being “coated” by glycerol (known to produce tangential surface anchoring²), which may also explain the long-term-stability of these platelets at the interface of polar glycerol and nonpolar LC. Colloidal assembly and defect transformations around spherical colloidal particles have recently attracted a great deal of attention because of the possibility of the chemo-responsive control of colloidal interactions that can be tuned from dipolar attractive to repulsive.^{29,30} The polygonal platelets used can produce weak director distortions of both dipolar and quadrupolar symmetry, however, they do not exhibit a well defined alignment with respect to the far-field director at the interface, because of the weak coupling of $\mathbf{n}(\mathbf{r})$ to the glycerol-submerged edge faces of the particles. However, the platelets at the interface of glycerol and a LC droplet with a concentric configuration of $\mathbf{n}(\mathbf{r})$ often tend to localize either in the center of the droplet (Fig. 5), a location of the surface point defect (the so-called boojum) induced by the geometry of the director pattern in the droplet, or next to the droplet’s contact line.

Our studies of biosynthesized gold platelets in the bulk and at the surfaces of the LCs suggest the possibility of

controlling surface boundary conditions for molecular alignment in LCs and may further expand the possible use of elasticity-mediated alignment,^{25,26,28} electrical and magnetic switching,^{26,28} and the assembly of complex-shaped particles in liquid crystals.²⁵ These self-alignment studies may be expanded to the case of other biosynthesized gold particles with anisotropic shapes, such as rods and ribbons (Figs. 1 and 6). In particular, rod-shaped gold colloids that induce tangential surface anchoring boundary conditions for the LC have been observed to align along the far-field director, which is consistent with observations in the literature.^{28,31} Possible applications of LC-gold nanoparticle composites include the design and fabrication of self-assembled optical metamaterials and the enhancement of conversion efficiencies of solar energy to electricity in organic-inorganic hybrid solar cells.^{25,26,28,30,32–36}

B. Shape stability of nanoparticles

Since particles of different sizes and shapes are naturally produced by different solvent conditions, it is important to consider the effects of changing solvents when preparing

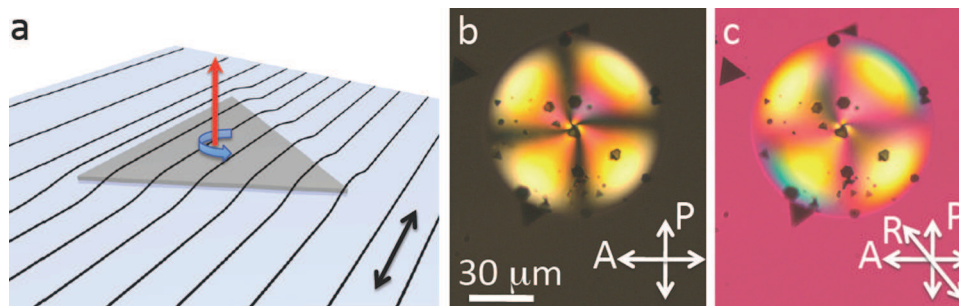


FIG. 5. (Color online) Gold polygonal platelets at the thermotropic LC-glycerol interface. (a) A schematic showing a platelet partially submerged in glycerol that induces tangential surface boundary conditions for $\mathbf{n}(\mathbf{r})$ and barely perturbs the uniform director structure; since the free energy cost of rotations around the red axis orthogonal to the platelet is small, the platelets are found at various possible orientations of their edges with respect to $\mathbf{n}(\mathbf{r})$. (b) and (c) Polarizing optical microscopy textures obtained for a sample between crossed polarizer “P” and analyzer “A,” (b) without, and (c) with an additional retardation plate with the fast axis marked “R;” the platelets within and outside of the area covered by a small LC droplet display arbitrary orientations of edge faces while having their large-area faces parallel to the LC-glycerol interface.

LC-nanoparticle composites. This is especially important since the redispersion of these nanoparticles into LCs often requires involving intermediate solvents. We observe that, upon phase transfer, single nanoparticles can change their shape and maintain their size or retain both shape and size (Fig. 6). For example, the methanol synthesized microtriangles are stable for several days in water, glycerol [Fig. 6(d)], and chromonic LCs. The shapes of methanol-synthesized gold platelets are also short-term stable (for about one day, typically becoming somewhat rounded after several days and eventually spherical) in the bulk of the thermotropic and rather nonpolar E31 nematic mixture. However, transferring 300 nm by 3–8 nm equilateral triangular platelets¹⁸ [Figs.

1(a) and 1(b)] from water into ethanol results in the formation of 400–700 nm \times 20 nm rods [Figs. 6(a) and 6(b)]. These rods have similar volumes to the starting nanotriangles, which suggests individual particle-to-particle shape transformations. The fact that the particles become rods of a different size than the rods directly obtained via synthesis in ethanol further supports the hypothesis that this is an individual particle transformation process.

Transferring particles from toluene to ethanol appears to produce ribbons [see the inset of Fig. 6(c)]. We have used scanning electron microscopy to obtain insights into the process of the formation of these ribbons. Similarly to the process described in the literature,³⁷ we see that at the onset of the ribbon formation, several spheres assemble in an anisotropic fashion to eventually transform into the ribbon [Fig. 6(c)]. Although the apparent shape plasticity of some of the used biosynthesized nanoparticle systems may be a limitation from a device development standpoint (since well-defined shapes easily change with changing solvents), it can also be purposefully utilized in the design of structured composites, provided that these shape transformations are well understood and controlled.

IV. CONCLUSIONS

To conclude, we have demonstrated that biosynthesized particles of desired shapes can be dispersed in liquid crystal host fluids and can impose well-defined vertical or tangential surface boundary conditions for the molecular alignment. These well-defined tangential or vertical boundary conditions, in turn, allow for achieving several different types of controlled long-range self-alignment of the anisotropic colloids in the bulk of the LCs, directed by the long-range orientational order of these anisotropic fluids that are of interest for the design of novel composite materials and metamaterials.^{25,26,28,36} We also show that the biosynthesized aloe vera capped nanoparticles show extraordinary shape plasticity as a function of the solvent but can also be dispersed in certain liquid crystalline and other solvents without the shape transformation.

ACKNOWLEDGMENTS

We thank N.A. Clark, B. Dan, D. Gardner, Q. Liu, A. Martinez, and B.I. Senyuk for helpful discussions. We

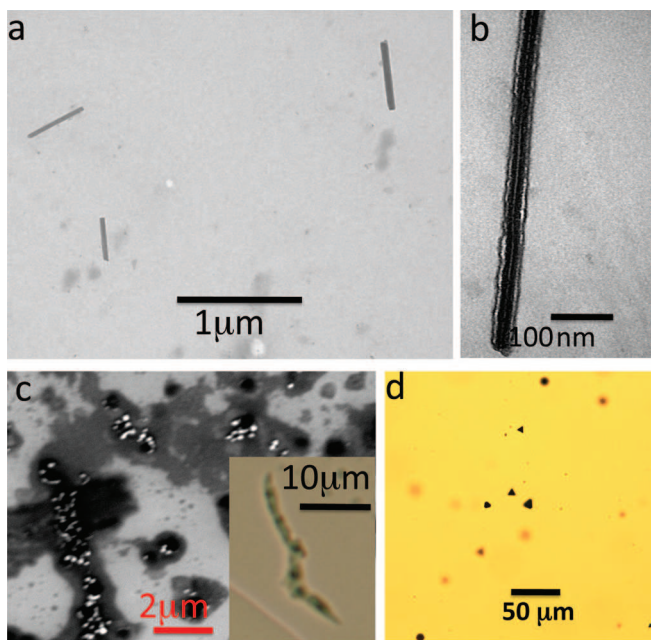


FIG. 6. (Color online) Post-synthetic shape stability of gold particles in different solvents. (a) A TEM image of 700 nm \times 20 nm rods obtained by redispersing 300 nm triangular platelets in ethanol. (b) A high-magnification TEM image of a single 700 nm \times 20 nm rod showing a well-pronounced line along its center. (c) A SEM image showing colloidal gold spheres originally obtained in toluene that aggregate in an anisotropic fashion when redispersed in ethanol to eventually produce ribbons (of which an optical micrograph is shown in the inset). (d) Optical micrograph showing that the shape of the polygonal colloidal platelets remains intact when the platelets are redispersed from methanol to glycerol.

acknowledge the support of the International Institute for Complex Adaptive Matter, CO Renewable and Sustainable Energy Initiative, the University of Colorado Innovation Seed Grant Program, and the National Science Foundation Grant Nos. DMR-0820579, DMR-0844115, and DMR-0847782.

- ¹P. Poulin, H. Stark, T. C. Lubensky, and D. A. Weitz, *Science* **275**, 1770 (1997).
- ²H. Stark, *Phys Rep.* **351**, 387 (2001).
- ³P. Poulin and D. A. Weitz, *Phys. Rev E* **57**, 626 (1998).
- ⁴C. L. van Oosten, C. W. M. Baastiansen, and D. J. Broer, *Nature Mater.* **8** 677 (2009).
- ⁵I. I. Smalyukh, A. V. Kachynski, A. N. Kuzmin, and P. N. Prasad, *Proc. Natl. Acad. Sci. U.S.A.* **103**, 18048 (2006).
- ⁶Y. Gu and N. L. Abbott, *Phys. Rev. Lett.* **85**, 4719 (2000).
- ⁷C. D. Santangelo and R. D. Kamien, *Phys. Rev. Lett.* **91**, 045506-1 (2003).
- ⁸S. J. Woltman, D. G. Jay, and G. P. Crawford, *Nature Mater.* **6**, 929 (2007).
- ⁹J. Yamamoto and H. Tanaka, *Nature Mater.* **4**, 75 (2005).
- ¹⁰I. I. Smalyukh, Y. Lansac, N. Clark, R. Trivedi, *Nature Mater.* **9**, 139 (2010).
- ¹¹N. Engheta, *Science* **317**, 1698 (2007).
- ¹²V. G. Veselago, *Sov. Phys. Usp.* **10**, 509 (1968).
- ¹³D. A. Pawlak, S. Turczynski, M. Gajc, K. Kolodziejak, R. Diduszko, K. Rozniatowski, J. Smalc, and I. Vendik, *Adv. Funct. Mater.* **20**, 1116 (2010).
- ¹⁴J. B. Pendrey, *Phys. Rev. Lett.* **85**, 3966 (2000).
- ¹⁵M. Brust, M. Walker, D. Bethell, D. Schiffrin, and R. Whyman, *J. Chem. Soc., Chem. Commun.* **801** (1994).
- ¹⁶C. Murphy, T. Sau, A. Gole, C. Orendorff, J. Gao, L. Gou, S. Hunyadi, and T. Li, *J. Phys. Chem. B* **109**, 13857 (2005).
- ¹⁷M. Grzelezak, J. Juste, P. Mulvaney, and L. Liz-Marzan, *Chem. Soc. Rev.* **37**, 1783 (2008).
- ¹⁸S. Chandran, M. Chaudhary, R. Pasricha, A. Ahmad, and M. Sastry, *Biotechnol. Prog.* **22**, 577 (2006).
- ¹⁹J. Xie, J. Y. Lee, and D. Y. C. Wang, *J. Phys. Chem. C* **111**, 10226 (2007).
- ²⁰S. Shankar, A. Rai, B. Ankamwar, A. Singh, A. Ahmad, and M. Sastry, *Nature Mater.* **3**, 482 (2004).
- ²¹Z. Li, A. Friedrich, and A. Taubert, *J. Mater. Chem.* **18**, 1008 (2007).
- ²²S. Stoeva, V. Zaikovski, B. Prasad, B. Stoimenov, C. Sorensen, and K. Klabunde, *Langmuir* **21**, 10280 (2005).
- ²³C. Lofton and W. Sigmund, *Adv. Funct. Mater.* **15**, 1197 (2005).
- ²⁴M. Zapotocky, L. Ramos, P. Poulin, T. C. Lubensky, and D. A. Weitz, *Science* **283**, 209 (1999).
- ²⁵C. Lapointe, T. Mason, and I. I. Smalyukh, *Science* **326**, 1083 (2009).
- ²⁶C. Lapointe, S. Hopkins, T. G. Mason, and I. I. Smalyukh, *Phys. Rev. Lett.* **105**, 178301 (2010).
- ²⁷T. Yamamoto, Y. Tabe, and H. Yokoyama, *Colloids Surf., A* **334**, 155 (2009).
- ²⁸Q. Liu, Y. Cui, D. Gardner, X. Li, S. He, and I. I. Smalyukh, *Nano Lett.* **10**, 1347 (2010).
- ²⁹G. M. Koenig, I.-H. Lin, and N. L. Abbott, *Proc. Natl. Acad. Sci. U.S.A.* **107**, 3998 (2010).
- ³⁰I. I. Smalyukh, *Proc. Natl. Acad. Sci. U.S.A.* **107**, 3945 (2010).
- ³¹I. I. Smalyukh, J. Butler, J. D. ShROUT, M. R. Parsek, and G. C. L. Wong, *Phys. Rev. E* **78**, 030701(R) (2008).
- ³²T. H. Reilly III, R. C. Tenent, T. M. Barnes, K. L. Rowlen, and J. van de Lagemaat, *ACS Nano* **2**, 615 (2010).
- ³³J. C. Johnson, T. H. Reilly III, A. C. Kanarr, and J. van de Lagemaat, *J. Phys. Chem. C* **113**, 6871 (2009).
- ³⁴H. A. Atwater and A. Polman, *Nature Mater.* **9**, 205 (2010).
- ³⁵M. J. Romero, A. J. Morfa, T. H. Reilly III, J. van de Lagemaat, and M. Al-Jassim, *Nano Lett.* **9**, 3904 (2009).
- ³⁶M. R. Jones, R. J. Macfarlane, B. Lee, J. Zhang, K. L. Young, A. J. Senesi, and C. A. Mirkin, *Nature Mater.* **9**, 913 (2010).
- ³⁷Y. Tan, J. Lee, and D. Wang, *J. Phys. Chem. C* **112**, 5463 (2008).